

STRENGTH OF CORONAL MASS EJECTION-DRIVEN SHOCKS NEAR THE SUN AND THEIR IMPORTANCE IN PREDICTING SOLAR ENERGETIC PARTICLE EVENTS

CHENGLONG SHEN,^{1,2} YUMING WANG,^{1,3,4} PINZHONG YE,^{1,2} X. P. ZHAO,⁵ BIN GUI,¹ AND S. WANG¹

Received 2007 April 18; accepted 2007 July 15

ABSTRACT

Coronal shocks are important structures, but there are no direct observations of them in solar and space physics. The strength of shocks plays a key role in shock-related phenomena, such as radio bursts and solar energetic particle (SEP) generation. This paper presents an improved method of calculating Alfvén speed and shock strength near the Sun. This method is based on using as many observations as possible, rather than one-dimensional global models. Two events, a relatively slow CME on 2001 September 15 and a very fast CME on 2000 June 15, are selected to illustrate the calculation process. The calculation results suggest that the slow CME drove a strong shock, with Mach number of 3.43–4.18, while the fast CME drove a relatively weak shock, with Mach number of 1.90–3.21. This is consistent with the radio observations, which find a stronger and longer decameter-hectometric (DH) type II radio burst during the first event, and a short DH type II radio burst during the second event. In particular, the calculation results explain the observational fact that the slow CME produced a major solar energetic particle (SEP) event, while the fast CME did not. Through a comparison of the two events, the importance of shock strength in predicting SEP events is addressed.

Subject headings: acceleration of particles — shock waves — Sun: coronal mass ejections (CMEs)

1. INTRODUCTION

Shock waves in the corona and interplanetary (IP) medium are usually generated when the speeds of coronal mass ejections (CMEs) exceed the local magnetosonic wave speed. Shocks particularly interest researchers, since they are not only associated with violent eruptions from the Sun, but may also have the ability to strongly accelerate particles, thereby leading to many effects that may significantly influence geo-space. For example, gradual solar energetic particle (SEP) events, one of the major space weather effects, are formed as the flux of energetic particles near the Earth exceeding a threshold. Most such energetic particles are thought to be generated at CME/interplanetary CME (ICME)-driven shocks (Cane et al. 1981; Reames 1999; Cane & Lario 2006). Type II radio bursts, another significant phenomenon in the corona and IP space, are excited by energetic electrons, which also generally accelerated by shocks (e.g., Nelson & Melrose 1985). The ability to accelerate particles is a distinct feature of shocks that could be rated by shock strength (e.g., Jones & Ellison 1991). Except for those IP shocks arriving at 1 AU and recorded by in situ spacecraft, many shocks of interest, e.g., the coronal shocks within about 5 solar radii, are far away from the observers and only have remote measured data. Thus, an accurate method for deducing shock strength is indispensable to understanding the physical processes involved in shock acceleration of particles and other related phenomena.

Up to now, all coronal shocks have been identified based on remote-sensing data. They can be discerned, for example, from

white-light images of corona from Large Angle Spectrometric Coronagraph (LASCO; Brueckner et al. 1995) on board the *Solar and Heliospheric Observatory* (SOHO), as done by Vourlidas et al. (2003), or from UV spectra observations obtained by the SOHO Ultraviolet Coronagraph Spectrometer (UVCS; Kohl et al. 1995) (e.g., Raymond et al. 2000; Mancuso et al. 2002; Raouafi et al. 2004; Ciaravella et al. 2005, 2006). So far, tens of coronal shocks have been identified in UVCS spectra. However, the best signature or indicator of coronal and IP shocks is still the decameter-hectometric (DH) to kilometeric type II radio bursts (call type IIs for short), which have been known for decades. Type IIs provide information about the plasma density at shocks, and seem to be essential to estimating shock speed and strength (e.g., Mancuso et al. 2002; Mann et al. 2003; Vršnak et al. 2004; Warmuth & Mann 2005).

The strength of a shock can be described by the fast-mode magnetosonic Mach number $M_{\text{ms}} = (V_{\text{sh}} - V_{\text{sw}})/V_{\text{ms}}$, where V_{sh} is the speed of a shock, V_{sw} is the background solar wind speed, $V_{\text{ms}} = [(V_A^2 + C_s^2 + |V_A^2 - C_s^2|)/2]^{1/2}$ is the fast-mode magnetosonic speed assuming that the wavevector is along the magnetic field lines, V_A is the Alfvén speed, and C_s is the sound speed. The Alfvén speed is defined as $V_A = B(\mu\rho)^{-1/2}$, where B is the strength of the background magnetic field and ρ is the background plasma density. Thus the values of V_{sh} , V_{sw} , V_A , and C_s are required to calculate the shock strength. The V_{sh} can be estimated according to the propagation of CMEs in the LASCO field of view (FOV) (see § 2). The V_{sw} is generally about 150 km s^{-1} at $5 R_{\odot}$, the solar radius, and even smaller below that height (Sheeley et al. 1997). Therefore, in most cases, V_{sw} could be ignored for a shock within $5 R_{\odot}$, because the speeds of shock-associated CMEs may reach several hundreds or even thousands of km s^{-1} at $2 R_{\odot}$. The Alfvén speed V_A depends on the magnetic field and plasma density, and C_s is related to the temperature. As to temperature, an isothermal atmosphere is a good approximation, because the coronal temperature is typically of the order of 10^6 K throughout IP space. Finally, two parameters, magnetic field and plasma density, are left unresolved.

¹ CAS Key Laboratory of Basic Plasma Physics, School of Earth and Space Sciences, University of Science and Technology of China, Hefei, Anhui 230026, China; ymwang@ustc.edu.cn, clshen@mail.ustc.edu.cn.

² State Key Laboratory of Space Weather, Chinese Academy of Science, Beijing, 100080, China.

³ Department of Computational and Data Sciences, George Mason University, Fairfax, VA 22030.

⁴ Corresponding author.

⁵ W. W. Hansen Experimental Physics Laboratory, Stanford University, Stanford, CA 94305.

Due to the lack of direct observations of magnetic field and plasma density, (quasi-) one-dimensional global models of magnetic field and density are widely used by researchers. For magnetic field, the simplest 1D model of magnetic field is described as $B(r) = B_{\odot}(R_{\odot}/r)^2$, based on the magnetic field conservation $B(r)r^2 = \text{const}$, in which $B_{\odot} = 2.2$ G is the magnetic field strength at solar surface $R = R_{\odot}$. To integrate some features of active regions, the model is sometimes modified by superimposing a magnetic dipole for active regions as adopted by e.g., Mann et al. (2003). There are also some 1D global models for plasma density, such as the Saito model (Saito et al. 1977), the Newkirk model (Newkirk 1961), and combinations of them (e.g., Gopalswamy et al. 2001). Combined with type II dynamic spectra, these density models could be used to deduce the height and speed of shocks. The fatal flaw of these models is also obvious. These models are highly ideal, and cannot resolve the variation in either the plane perpendicular to the radial direction or in the temporal plane, which is probably significant, as seen in § 3 for the variation of magnetic field strength, and in Cho et al. (2007) for density.

In this paper we present an improved method for calculating the coronal Alfvén speed and shock Mach number above $2 R_{\odot}$ by investigating two CME events. In our method, a more realistic model is used to extrapolate the coronal magnetic field based on photospheric measurements, DH type II observations are analyzed to obtain the density at shocks, and CME snapshots recorded by coronagraphs are adopted to estimate height information. The two events selected to illustrate the calculation process are a fast CME without a major SEP event and a relatively slow CME causing a major SEP event. In this paper, a major SEP event is defined following NOAA's criterion that the peak intensity of proton flux with energy >10 MeV observed at the near Earth space exceeds 10 pfu (particles $\text{cm}^{-2} \text{s}^{-1} \text{sr}^{-1}$), which is also widely used by many other researchers. As will be seen, the calculation results are consistent with observations. In particular, the two studied events confirm the importance of shock strength in predicting SEP events. The two events are counterexamples to the suggestion that faster CMEs produce larger SEP events. Our derived shock Mach numbers for the two events explain the unusual phenomena. The next section will introduce the calculation process step by step. In § 3, the two events are presented to further illustrate the method. A comparison of the two events with respect of SEP intensity is given in § 4. Finally, in § 5, we summarize the paper and offer a brief discussion.

2. OUR METHOD

Step 1: Calculation of the local plasma density using the dynamic spectra of DH type II bursts.—Solar radio bursts of type II are indicative of shocks propagating in the corona and heliosphere accompanied by electron acceleration (Malitson et al. 1973; Wild & McCready 1950; Holman & Pesses 1983). They are thought to be produced in the upstream plasma rather than in the denser downstream plasma, and their frequency reflects the local electron density (Dulk et al. 1971; Holman & Pesses 1983). Therefore, type IIs can be used to deduce the density of the ambient plasma that shocks are passing through. Type IIs usually have fundamental (F) and harmonic (H) components. The fundamental component is emitted at the place where the wave frequency is equal to the local electron plasma frequency. From the frequency of the type IIs fundamental component, we can calculate the local electron number density through $N_e = [f_{pe}(\text{Hz})/(8.98 \times 10^3)]^2 \text{cm}^{-3}$. Considering the presence of multiple species, the following relationship between the electron number density and the plasma density in

the solar corona suggested by Priest (1982) is used to calculate the plasma density:

$$\rho = 1.92 \tilde{\mu} m_p N_e = 1.92 \tilde{\mu} m_p \left[\frac{f_{pe}(\text{Hz})}{8.98 \times 10^3} \right]^2 \text{cm}^{-3}, \quad (1)$$

where m_p is proton mass, with mean molecular weight $\tilde{\mu} = 0.6$ (Priest 1982).

In this paper, we study the ambient conditions and the coronal shocks only in the DH frequency range, because (1) the DH frequency range (~ 1 – 14 MHz) corresponds to the heliocentric distance, ~ 2 – $10 R_{\odot}$, where CME-driven shocks are thought to be most efficient for energetic particle generation (Kahler 1994; Cliver et al. 2004); and (2) the DH type IIs are thought to be produced at the noses of shocks, unlike the metric type IIs, whose source regions are not clear (e.g., Gary et al. 1984; Maia et al. 2000; Gopalswamy et al. 1997; Cho et al. 2007; Robinson & Stewart 1985; Klein et al. 1999; Gopalswamy & Kaiser 2002). The spaceborne instrument, *Wind/Waves* (Bougeret et al. 1995) monitors radio emissions in this frequency range, and could be used to deduce the local plasma density.

The *SOHO/LASCO* C2 and C3 cameras give the time sequence of the CME propagation from 1.5 to $30 R_{\odot}$. This can be used to measure the height-time (HT) curve of a CME, and read the projected heliocentric distance and speed of the CME leading front at any given time. Following Gopalswamy et al. (2005) and Cho et al. (2005), we assume that (1) DH type II radio bursts are generated at the front of CME-driven shocks, and (2) the shock standoff distance is relatively small near the Sun, and therefore can be ignored. For metric type IIs, many 2D radio images show that metric type II sources are behind the CME fronts (Robinson & Stewart 1985; Klein et al. 1999). One possible explanation is that the shocks resulting in metric type IIs are located at the flanks of CMEs due to their expansion (e.g., Gopalswamy & Kaiser 2002). However, type IIs with longer wavelength are thought to originate ahead of the CME fronts, because CMEs propagate forward and shocks will be driven ahead of them. Thus, the first assumption, which is also mentioned in the step 1, is reasonable. The second assumption is also acceptable, since there is some evidence that the CME bright leading edges are probably shock fronts (e.g., Vourlidis et al. 2003; Ciaravella et al. 2006). Under these assumptions, CME leading fronts may act as a proxy of shocks and therefore be related to DH type IIs. We also assume that CMEs propagate radially, and correct every measured height, H_{meas} , in 2D LASCO images to the heliocentric distance, H_{dhelio} , by the equation

$$H_{\text{dhelio}} = \frac{H_{\text{meas}}}{\sqrt{(\cos \theta \sin \phi)^2 + \sin^2 \theta}}, \quad (2)$$

where θ is the latitude and Φ is the longitude of the source region of a CME, which is determined by examining *SOHO/EIT* (Extreme Ultraviolet Imaging Telescope; Delaboudiniere et al. 1995) movies. Then we fit the HT scatter plot with a second-order polynomial to get the real CME trajectory. To assess how good the approximation is, we extrapolate the fitted curve down to the solar surface, $H_{\text{dhelio}} = 1 R_{\odot}$, where a CME originates, and compare the extrapolated CME onset time, T_{OL} , with the observed onset time, T_{OE} , defined as the first appearance of the CME-related eruptive activity in EIT images. A small difference between T_{OE} and T_{OL} indicates a good approximation, since the cadence of EIT data is only about 12 minutes.

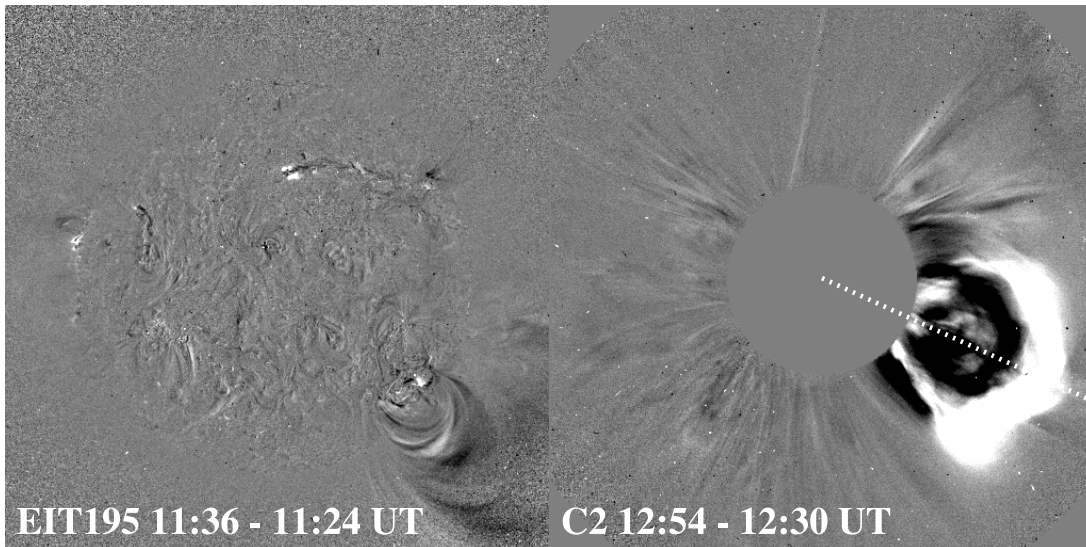


FIG. 1.—EIT and LASCO running-difference images of 2001 September 15 event. The dashed line indicates the direction along which the heights of the CME front were measured.

Step 3: Calculation of the background magnetic field strength at the shock by the CSSS model.—Up to now, there have been no observations of 3D magnetic field in the corona. Most of our information about coronal magnetic field comes from extrapolation with the aid of models, such as the potential field source surface model (PFSS; Schatten et al. 1969; Altschuler & Newkirk 1969), the potential field-current sheet model (PFCS; Schatten 1971), the horizontal current-source surface model (HCCS; Zhao & Hoeksema 1992), the horizontal current-current sheet model (HCCS; Zhao & Hoeksema 1994), the current sheet-source surface model (CSSS; Zhao & Hoeksema 1995; Zhao et al. 2002), and so on. These models, in which the measured photospheric longitudinal magnetic field is input as the bottom boundary, are more robust and complicated than the 1D global models mentioned in the introduction. The extrapolated magnetic fields usually match well the large-scale features observed at other wavelengths (Schrijver et al. 2005).

In this paper, the mature CSSS model is used to extrapolate the coronal magnetic field. The bottom boundary is adopted from the WSO (Wilcox Solar Observatory) synoptic charts,⁶ which are assembled from individual magnetograms observed over a Carrington rotation. Previous work by Zhao and colleagues has shown that the extrapolated magnetic field can approximately reproduce the observed variation of magnetic field in latitude and values at 1 AU (Zhao & Hoeksema 1995; Zhao et al. 2002). In our study, the strength of the magnetic field at the shock is an average of the extrapolated magnetic field over a circular region of radius 10° at the height where the DH type II emitted, above the CME source region. Note that the extrapolated magnetic field is an average over a Carrington rotation, and will not exactly reflect the state at the time of interest. However, since our study is interested in large-scale phenomena and non-CME-disturbed magnetic field, we think the averaged state will not significantly distort our results; nevertheless, we take an error of 20% in magnetic field strength into account in order to make our calculation results more reliable.

Step 4: Calculation of the Alfvén speed and fast-mode magnetosonic Mach number.—From steps 1–3, the background plasmas density (ρ), the height and speed of the shock (V_{sh}), and the

magnetic field strength (B) are deduced independently. As discussed in § 1, we ignore the background solar wind speed and assume an isothermal corona with $T = 1.4$ MK, which corresponds to a constant C_s of 180 km s^{-1} . Therefore, the Alfvén speed and the fast-mode magnetosonic Mach number indicating the shock strength can be calculated.

3. TWO CASES

3.1. 2001 September 15 Event

Figure 1 shows the running difference images from *SOHO*/EIT and LASCO for this CME. The CME was first observed by LASCO/C2 at 11:54 UT on 2001 September 15. It looks like a bright bubble traveling along the southwest direction in the C2 FOV, as shown in the right panel of Figure 1. The EIT image (*left panel*) shows that the source region of this CME is at about $S27^\circ$, $W48^\circ$, above which a large EUV dimming and opening of loops could be seen. EIT images and the soft X-ray profile from the *GOES* satellite (Fig. 2, *dotted line*) indicate that the CME was associated with an M1.5 flare. The significant eruptive signatures in the source region first appeared in the 11:12 UT (T_{OE}) EIT image. By combining the images taken by the C2 and C3 cameras, we measure the HT profile of the leading front of this CME until it fades into background. The direction of the measurement is chosen artificially, but lies mainly along the center of the major part of the CME, as indicated by the dashed line in Figure 1. The measured heights are further corrected by equation (2), and are shown by the cross (from C2 measurements) and asterisk (from C3 measurements) in Figure 2. Through a second-order polynomial fitting, the heliocentric distance of the CME front as a function of time is obtained. The acceleration is estimated as -12.72 m s^{-2} , and the CME speed decreases from 772 km s^{-1} at $2 R_\odot$ to 674 km s^{-1} at $10 R_\odot$. From the fitting curve in Figure 2, the extrapolated onset time, T_{OL} , of the CME is about 11:09 UT. The difference between T_{OL} and T_{OE} is only 3 minutes, indicating that this fitted HT profile is a good approximation to reality.

This CME was accompanied with a clear DH type II radio burst observed by the *Wind*/Waves, as shown in Figure 3. Since there were no other faster CMEs occurring near the CME of interest, the association between the DH type II and the CME is definite. The beginning and end times of this DH type II event have

⁶ See <http://wso.stanford.edu/synoptical.html>.

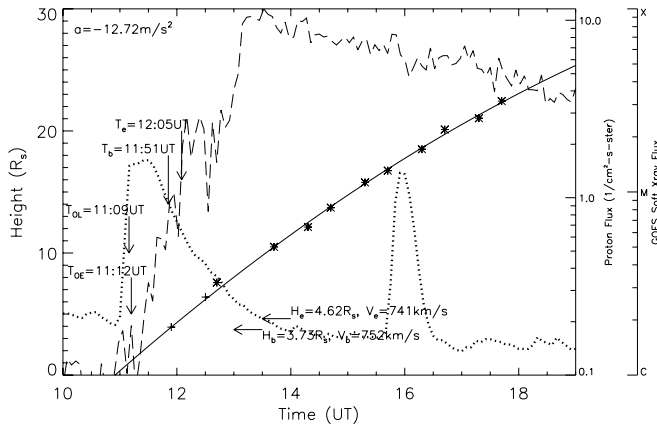


FIG. 2.—Heliocentric height-time plot of 2001 September 15 CME. The cross and asterisk denote the C2 and C3 measurements, respectively. The solid line is the second-order polynomial fitting line. T_{OL} denotes the extrapolated CME onset time. T_{OE} is the observed CME onset time in EIT images. T_b denotes the begin time of the associated DH type II, and H_b and V_b denote the height and speed of the CME front at that time. T_e denotes the end time of the DH type II, and H_e and V_e are the corresponding height and speed of the CME front. The dashed profile shows the flux of energetic protons with energy larger than 10 MeV observed by *GOES*. A 1 hr flight time of protons from the Sun to 1 AU has been deducted from the proton flux profile by assuming zero scattering in the interplanetary space. The dotted line denotes the *GOES* soft X-ray flux at the wavelength of 1.0–8.0 Å.

been marked by T_b and T_e in Figure 2. The main emission from 11:51 UT (T_b) to 12:05 UT (T_e) is the fundamental; the harmonic appears only at the very top of the detectable frequency range, near the end of the event (M. L. Kaiser 2006, private communication). Since the fundamental frequency is diffused in a range, two white dashed lines are used to denote its upper and lower limits. At the beginning of the event, the frequency covers the approximate range from 11.06 to 13.07 MHz, which corresponds to the plasma density range from 2.91×10^{-18} to $4.06 \times 10^{-18} \text{ g cm}^{-3}$. Both values are used in the subsequent calculation of V_A , V_{ms} , and M_{ms} for upper and lower limits. The heliocentric distance and speed of the CME are independently estimated as $3.73 R_\odot$ and 752 km s^{-1} at T_b , and $4.62 R_\odot$ and 741 km s^{-1} at T_e .

As outlined in § 2, extrapolation of the coronal magnetic field is performed using the CSSS model, based on the WSO synoptic chart of Carrington rotation 1980, corresponding to the period from 13:38 UT 2001 August 23 to 19:51 UT 2001 September 19. Figure 4 shows the strength distribution of the extrapolated magnetic field at height $3.73 R_\odot$, where the DH type II has just started. We find that the magnetic field strength varies over a large range from 0.03 to 0.12 G, which indicates that Alfvén speeds at a given altitude could be quite different, which directly influences the formation and strength of shocks. The enclosed region right above the CME source region is treated as an effective region, where the DH type II burst is emitted. The mean strength of the magnetic field at this height in this region is 0.11 G.

Combining the magnetic field strength with the plasma density, the Alfvén speed and fast-mode magnetosonic speed are calculated as $124\text{--}219 \text{ km s}^{-1}$ and $180\text{--}219 \text{ km s}^{-1}$, respectively, at the beginning of the DH type II. Therefore, the shock strength of the CME, indicated by the fast-mode magnetosonic Mach number, is 3.43–4.18. The ranges of these values include the possible 20% error in the extrapolated magnetic field. Usually a shock with Alfvén Mach number larger than 2.7 is a supercritical shock, such as the bow shock ahead of the magnetosphere of the Earth, while many interplanetary shocks are subcritical. The fact that the coronal shock driven by the CME on 2001 September 15 has a fast-mode magnetosonic Mach number larger than 3.43 means that,

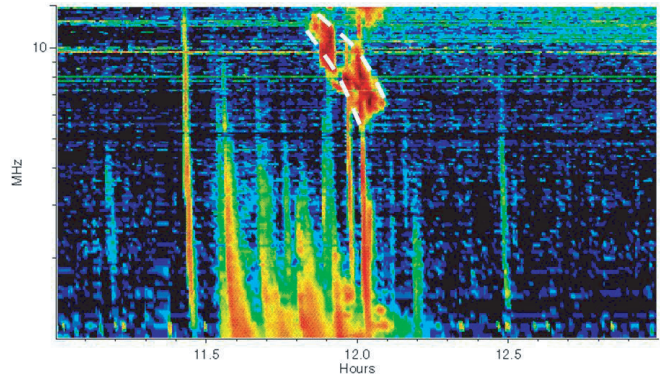


FIG. 3.—*Wind/Waves* observations during 11:00–13:00 UT on 2001 September 15. The dashed lines denote the frequency range of the fundamental component of a DH type II.

although the shock driver was not so fast, the shock was indeed strong and had the capacity to cause a strong DH type II burst, which was observed by *Wind/Waves*. Moreover, this strong shock also caused a major SEP event, in which the maximum proton flux intensity with energy >10 MeV observed by *GOES* was 11.6 pfu.

3.2. 2000 June 15 Event

The CME and its source region are presented in the running-difference LASCO and EIT images of Figure 5. This is a fast CME, first appearing at 20:06 UT on 2000 June 15 in LASCO/C2 and traveling along the northwest direction. It originated from $N19^\circ$, $W56^\circ$, where a sudden brightening could be found. An M1.9 class flare associated with this event could be identified from EIT images and the soft X-ray profile shown in Figure 6. The first eruptive signature recorded by EIT was at 19:36 UT. Figure 6 shows the HT scatter of the leading front of this CME, in which all measured heights have been corrected to the heliocentric distance, and the fitting curve by a second-order polynomial. By extrapolating the curve down to the solar surface, we find that the estimated onset time of the CME is 19:33 UT, close to the EIT onset time 19:36 UT. This indicates that the fitted result is a good approximation to reality. The acceleration of this CME was -64.54 m s^{-2} , and the speed was 1451 km s^{-1} at $2 R_\odot$ and 1176 km s^{-1} at $10 R_\odot$.

Figure 7 displays the *Wind/Waves* radio spectrum for this event. A DH type II radio burst from about 19:52 to 19:56 UT is found. This radio burst is in the *Wind/Waves* type II list.⁷ This DH type II radio burst is shorter, but has obvious fundamental and harmonic components. The fundamental began at about 19:52 UT around 2.4 MHz, and the harmonic appeared at about 5 MHz. We might expect that the related CME-driven shock should be weaker than

⁷ See <http://lep694.gsfc.nasa.gov/waves/waves.html>.

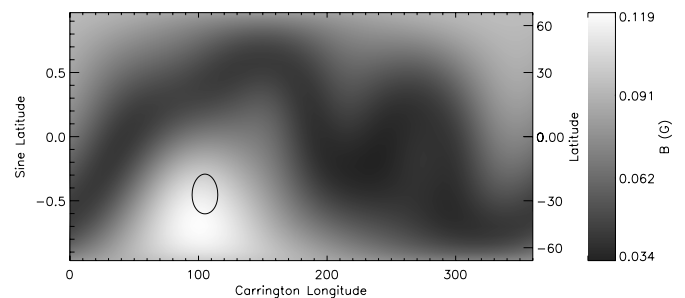


FIG. 4.—Distribution of the WSO CR 1980 extrapolated magnetic field strength at the height of $3.73 R_\odot$, where the DH type II began to emit.

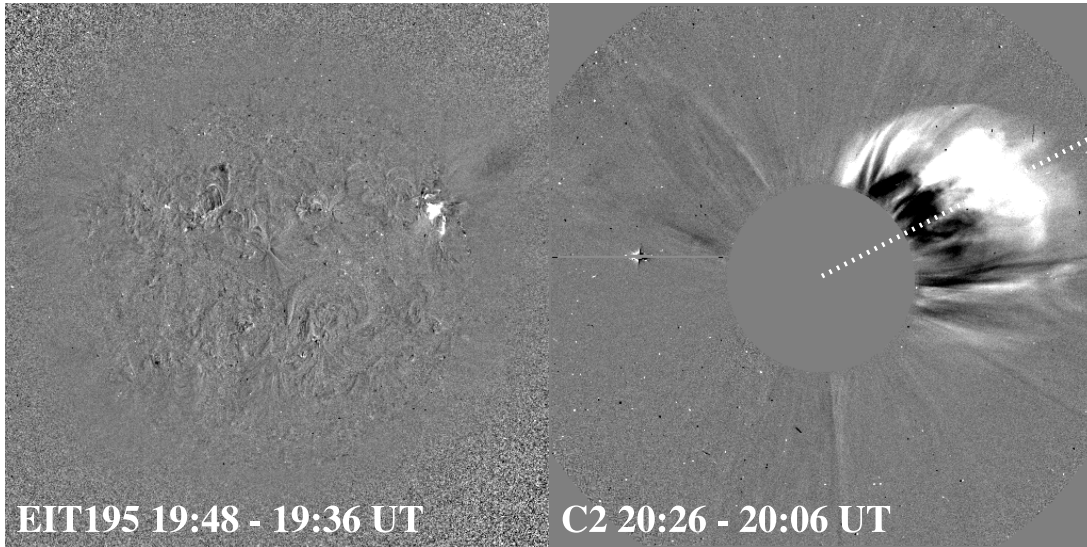


FIG. 5.—EIT and LASCO running-difference images of 2000 June 15 event.

the shock driven by the first CME, since the DH type II was weaker and shorter. The two dashed lines denote the upper and lower limits of the frequency of the fundamental component of this burst. At the beginning, $T_b = 19:52$ UT, the frequency of fundamental component extended in the range from ~ 2.24 to 2.52 MHz, which corresponds to a plasma density of $1.19\text{--}1.51 \times 10^{-19} \text{ g cm}^{-3}$ according to equation (1). From the fitting curve in Figure 6, the heliocentric distance and speed of the CME are $3.32 R_\odot$ and 1409 km s^{-1} at the start time, T_b , of the DH type II burst, and $3.80 R_\odot$ and 1393 km s^{-1} at the end time, T_e . It was thus much faster than the 2001 September 15 CME.

The WSO synoptic chart of Carrington rotation 1963, which covers the period from 03:06 UT 2000 May 17 to 08:17 UT 2000 June 13, is used to extrapolate the coronal magnetic field. We use the previous synoptic chart rather than the one covering the CME onset time, because the time of the CME source region passing across the central meridian is in Carrington rotation 1963. Figure 8 shows the strength distribution of the magnetic field at $H = 3.32 R_\odot$, where the DH type II began to emit. The magnetic field strength varies from 0.033 to 0.144 G, a larger range than that in the first event. The effective region above the CME source region is enclosed by the black circle in Figure 8. The mean magnetic field strength at this height in the effective region is 0.076 G.

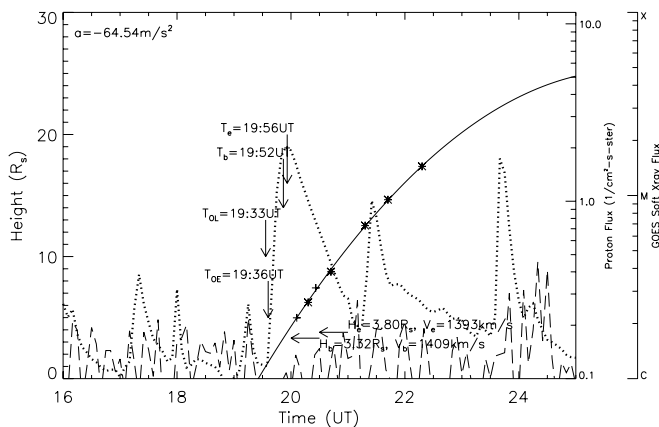


FIG. 6.—HT plot, proton flux profile, and soft X-ray profile of the 2000 June 15 event.

Our calculations give the values of Alfvén speed and fast-mode magnetosonic speed for this event as $439\text{--}741 \text{ km s}^{-1}$ and $439\text{--}741 \text{ km s}^{-1}$, respectively, at the beginning of the DH type II. Therefore, the shock strength, M_{ms} , of the CME is $1.90\text{--}3.21$. The smaller Mach number indicates that the shock was relatively weak, as expected. The lower limit of M_{ms} , 1.90, indicates that the shock may be so weak that it just exceeds the critical condition (Mach number 1.6) of a shock generating suprathermal electrons (Mann et al. 1995).

4. COMPARISON OF THE CASES: SEP FLUX

Fast CMEs are usually thought to be a good producer of SEP events, since they generally drive a shock ahead (e.g., Kahler 2001; Lario 2005). It is also recognized that SEP events are not always fully observable near Earth, even if a CME does generate them. This is because these energetic particles generally move along the spiral interplanetary magnetic field lines, and only the particles on the field lines connecting to the Earth will be recorded. Thus, fast CMEs originating from western hemisphere are thought to be more likely to cause an SEP event near Earth. As shown by Gopalswamy et al. (2004), 51 out of any 60 SEP events are caused by CMEs originating from the western solar hemisphere.

However, counterexamples exist, of fast CMEs that do not cause an SEP event and slow CMEs that do. We studied 56 fast (projected speed $\geq 1000 \text{ km s}^{-1}$) CMEs originating from the western

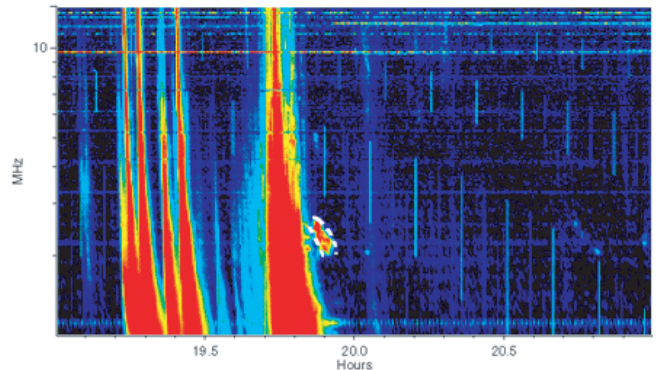


FIG. 7.—Wind/Waves observations during 19:00–21:00 UT on 2000 June 15.

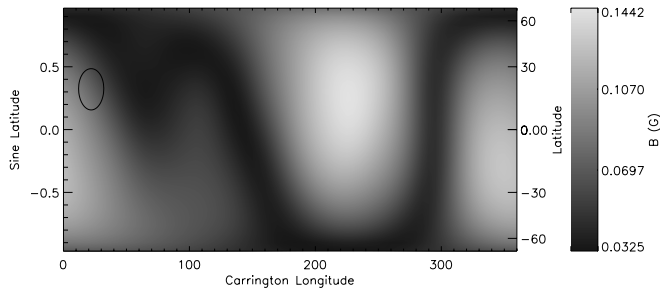


FIG. 8.—WSO CR 1963 extrapolated magnetic field strength at the height of $3.32 R_{\odot}$, where the DH type II began to emit.

hemisphere during 1997–2003, and found that 12 CMEs did not cause any enhancement of energetic proton flux at proton energy ≥ 10 MeV (Shen et al. 2006). Kahler & Vourlidas (2005) presented 16 SEP-poor fast CMEs with speeds above 1060 km s^{-1} . Reinard & Andrews (2006) also found 14 CMEs with speeds $\geq 1000 \text{ km s}^{-1}$ that did not cause an SEP event. One possible explanation is that the CME speed does not always reflect the real shock strength. The comparison of flux profiles of protons with energy larger than 10 MeV between the two events analyzed here illustrates this issue. Of course, there is an alternative explanation for slow events associated with SEPs—that the energetic particles do not come from shocks, but from some other source, such as flares. Such phenomena will not be addressed in this paper.

Our two events are summarized in Table 1, which lists the DH type II, CME location and speed, flare intensity, plasma density, magnetic field strength, Alfvén speed, fast magnetosonic speed, and fast magnetosonic Mach number, as well as the SEP intensity. Both CMEs originated from the western hemisphere in the almost same longitude, and were associated with similar flares of similar intensity (class of M1.5 and M1.9, respectively), so they are comparable.

The 2001 September 15 CME (number 1) is not a very fast CME. Its speed is 752 km s^{-1} , about half of that of the 2000 June 15 CME (number 2). Based only on the CME speeds, we might expect that CME 2 should produce a larger SEP event. However, in fact CME 2 did not produce a major SEP event, but CME 1 did, with peak SEP flux reaching 11.6 pfu (as listed in the last column of Table 1).

The flux profiles of the protons with energy larger than 10 MeV recorded by *GOES* are shown by the dashed lines in Figures 2 and 6. The *GOES* instrument has a high background, but this should not affect our results, since *GOES* proton flux profiles are mainly used to determine whether or not there was an SEP event. Assuming zero scattering of protons propagating in the interplanetary space, the proton flight time of about 1 hr from the Sun to 1 AU has been deducted from the proton flux profile. For CME 1, the proton flux increased soon after the CME onset, to a maximum value of 11.6 pfu . For CME 2, the proton flux profile fluctuates (comparable to the background noise) at the bottom of Figure 6 if scaled to the same scale as Figure 2, which suggests that there was no significant enhancement of the energetic proton flux. These observations are consistent with our calculated shock strengths, which indicate that CME 1 drove a stronger shock, although it was relatively slow, while CME 2 drove a relatively weak shock, although it was very fast.

5. CONCLUSION AND DISCUSSION

In this study, we present an improved method for calculating the Alfvén speed and shock strength near the Sun ($>2 R_{\odot}$), in which as many observations as possible are used. We use DH type II radio

TABLE 1
COMPARISON OF THE 2001 SEPTEMBER 15 AND 2000 JUNE 15 EVENTS

Parameter	2001 Sep 15	2000 Jun 15
DH Type II bursts:		
T_b (UT).....	11:51	19:52
F (MHz).....	11.06–13.07	2.24–2.52
CMEs:		
Location	S27°, W48°	N19°, W56°
H (R_{\odot}).....	3.73	3.32
V (km s^{-1}).....	752	1409
Flares.....	M1.5	M1.9
Derived Quantities:		
ρ ($10^{-18} \text{ g cm}^{-3}$).....	2.91–4.06	0.119–0.151
B (G).....	0.088–0.132	0.061–0.091
V_A (km s^{-1}).....	124–219	439–741
V_{ms} (km s^{-1}).....	180–219	439–741
M_{ms}	3.43–4.18	1.90–3.21
SEP (pfu).....	11.6	...

bursts instead of a 1D global density model to deduce the ambient plasma density, use LASCO and EIT images to deduce the heliocentric distance and shock speed at the time of DH type II bursts, and use WSO synoptic charts and CSSS models to extrapolate the coronal magnetic field. The plasma density, height and speed of shocks, and magnetic field strength are all deduced independently. Two events, a relatively slow CME on 2001 September 15 and a very fast CME on 2000 June 15, are chosen to describe the calculation process. The calculation results suggest that the first event had a stronger shock, with Mach number larger than 3.43 and up to 4.18, while the second event had a relatively weak shock, with Mach number less than 3.21 and as low as 1.90. Here we would like to emphasize the lower limit of the Mach number of the second shock, which is just above the critical point for a shock to generate superthermal electrons, as suggested by Mann et al. (1995). These results are consistent with the radio observations, which find a stronger and longer DH type II radio burst during the first event, and a shorter DH type II during the second event.

The two events are further compared with respect to SEP generation. We find that the first CME produced a major SEP event, although it is relatively slow, while the second CME did not cause a significant enhancement of energetic protons, although it is very fast. This also agrees with our calculations that the first CME drove a strong shock, while the second CME drove a weak shock. The consistency in the comparisons of our calculations with both radio emissions and SEP flux implies that the calculation method we proposed here is reliable. According to the LASCO CME catalog,⁸ the energy of the first CME was $\sim 6.0 \times 10^{30} \text{ erg}$, and that of the second CME was $\sim 3.1 \times 10^{31} \text{ erg}$. This means that neither speed nor kinematic energy correctly reflects the real strength of potential shocks. The importance of the accurate estimation of shock strength to the prediction of SEP events is therefore emphasized.

Table 2 highlights the differences between our calculations and those suggested by ideal models. For each event, the first row shows our calculated parameters, as given in Table 1, and the second row lists the plasma density given by the one-fold Newkirk model (Newkirk 1961), the magnetic field strength given by $B(r) = B_{\odot}(R_{\odot}/r)^2$ with $B_{\odot} = 2.2 \text{ G}$, and the corresponding fast-mode magnetosonic speed and Mach number. The results from ideal models suggest that the first CME should drive a relatively weak shock and the second CME drove a stronger shock. This is

⁸ Available at: http://cdaw.gsfc.nasa.gov/CME_list/.

TABLE 2
COMPARISON OF OUR RESULTS WITH IDEAL MODELS

Event	H (R_{\odot})	V (km s^{-1})	ρ ($10^{-18} \text{ g cm}^{-3}$)	B (G)	V_{ms} (km s^{-1})	M_{ms} (km s^{-1})
2001 Sep 15.....	3.73	752	2.91–4.06	0.088–0.132	180–219	3.43–4.18
Ideal models.....			1.17	0.16	413	1.82
2000 Jun 15.....	3.32	1409	0.119–0.151	0.061–0.091	439–741	1.90–3.21
Ideal models.....			1.62	0.20	442	3.19

opposite to our conclusion, and obviously contrary to the radio and SEP observations discussed above.

Why the slower CME should have driven a stronger shock can be answered from Table 1. The ambient plasma ahead of CME 1 from the DH type II burst is much denser than that ahead of CME 2, while their heights are almost the same. In ideal density models, the plasma density should decrease with increasing height. However, although the height in event 1 is $3.73 R_{\odot}$ higher than $3.32 R_{\odot}$ in event 2, the plasma density in event 1 is about 27 times of that in event 2. This is the main reason why the fast magnetosonic speed in event 1 is much smaller than that in event 2. In addition, note that the variation of density and magnetic field strength with time and/or location (even in the same altitude) is significant. The two studied events show that the density can vary over about one order of magnitude, and the magnetic field strength can also vary over a few orders (Figs. 4 and 8). Such large variations make it unreliable to use CME speed as a proxy for the shock strength.

SEPs are an important effect of space weather. In this paper, we only regard the peak intensity of energetic proton flux with energies larger than 10 MeV, one of the most studied issue in space weather research. Actually, SEP acceleration and its manifestation are very complicated even in the events we studied here. Although there was no significant enhancement of the proton flux in event 2, the enhancement of the electron flux (up to $\sim 10^5 \text{ particles cm}^{-2} \text{ s}^{-1} \text{ sr}^{-1} \text{ MeV}^{-1}$ for the energy range 38–53 keV) observed by the ACE/EPAM instrument was much larger than the $\sim 2 \times 10^4 \text{ particles cm}^{-2} \text{ s}^{-1} \text{ sr}^{-1} \text{ MeV}^{-1}$ in event 1, and the enhancements of heavy ions in event 2 were also larger than those in event 1. To fully address these phenomena requires knowledge of the sources of these energetic particles (they may come from different places, shocks, and/or flares), the acceleration preferences shown to spe-

cies under different acceleration mechanisms, and so on, which is beyond the scope of this paper.

Even so, how to predict the intensities of SEP events is still an interesting topic. Although it is well known that shock acceleration is the main mechanism of SEP generation, the correlation between shock strength and SEP intensity is still not well established. There is a general relationship between CME speed and SEP intensity, but the scatter is large (Reames 2000). One major reason for this is that the CME speed does not reflect the real strength of the CME-driven shock. In addition, based on our calculations, the presence of shocks does not seem to be a sufficient condition for SEP generation; there may also be a minimum threshold of strength, only above which will the shock be able to accelerate energetic protons efficiently. Thus, we are now extending our present work to a statistical study that should be of benefit to our understanding of proton acceleration by shocks and in space weather research.

We acknowledge the use of the data from the LASCO and EIT instruments on board *SOHO*, the *Wind/Waves* instrument, the *GOES* satellites, the *ACE/EPAM* instrument, and *WSO*. *SOHO* is a project of international cooperation between ESA and NASA. We thank Yihua Yan and Shujuan Wang for help in analyzing radio bursts. We are grateful to the referee's comments and suggestions. This work is supported by grants from the NSF of China (40574063, 40525014, 40336052, 40404014), the 973 project (2006CB806304), the Chinese Academy of Sciences (KZCX3-SW-144 and the startup fund), the Program for New Century Excellent Talents in University (NCET-04-0578), and the Ministry of Education (200530).

REFERENCES

- Altschuler, M. D., & Newkirk, G. 1969, *Sol. Phys.*, 9, 131
 Bougeret, J.-L., et al. 1995, *Space Sci. Rev.*, 71, 231
 Brueckner, G. E., et al. 1995, *Sol. Phys.*, 162, 357
 Cane, H. V., & Lario, D. 2006, *Space Sci. Rev.*, 123, 45
 Cane, H. V., Stone, R. G., Fainberg, J., Steinberg, J. L., Hoang, S., & Stewart, R. T. 1981, *Geophys. Res. Lett.*, 8, 1285
 Cho, K.-S., Lee, J., Moon, Y.-J., Dryer, M., Bong, S.-C., Kim, Y.-H., & Park, Y. D. 2007, *A&A*, 461, 1121
 Cho, K. S., Moon, Y. J., Dryer, M., Shanmugaraju, A., Fry, C. D., Kim, Y. H., Bong, S. C., & Park, Y. D. 2005, *J. Geophys. Res.*, 110, A12101
 Ciaravella, A., Raymond, J. C., & Kahler, S. W. 2006, *ApJ*, 652, 774
 Ciaravella, A., Raymond, J. C., Kahler, S. W., Vourlidas, A., & Li, J. 2005, *ApJ*, 621, 1121
 Cliver, E. W., Kahler, S. W., & Reames, D. V. 2004, *ApJ*, 605, 902
 Delaboudiniere, J.-P., et al. 1995, *Sol. Phys.*, 162, 291
 Dulk, G. A., Altschuler, M. D., & Smerd, S. F. 1971, *Astrophys. Lett.*, 8, 235
 Gary, D. E., Dulk, G. A., House, L., Illing, R., Sawyer, C., Wagner, W. J., McLean, D. J., & Hildner, E. 1984, *A&A*, 134, 222
 Gopalswamy, N., Aguilar-Rodriguez, E., Yashiro, S., Nunes, S., Kaiser, M. L., & Howard, R. A. 2005, *J. Geophys. Res.*, 110, A12S07
 Gopalswamy, N., & Kaiser, M. L. 2002, *Adv. Space Res.*, 29, 307
 Gopalswamy, N., Kundu, M. R., Manoharan, P. K., Raoult, A., Nitta, N., & Zarka, P. 1997, *ApJ*, 486, 1036
 Gopalswamy, N., Yashiro, S., Kaiser, S., Howard, R. A., & Bougeret, J.-L. 2001, *J. Geophys. Res.*, 106, 29219
 Gopalswamy, N., Yashiro, S., Krucker, S., Stenborg, G., & Howard, R. A. 2004, *J. Geophys. Res.*, 109, A12105
 Holman, G. D., & Pesses, M. E. 1983, *ApJ*, 267, 837
 Jones, F. C., & Ellison, D. C. 1991, *Space Sci. Rev.*, 58, 259
 Kahler, S. W. 1994, *ApJ*, 428, 837
 ———. 2001, *J. Geophys. Res.*, 106, 20947
 Kahler, S. W., & Vourlidas, A. 2005, *J. Geophys. Res.*, 110, A12S01
 Klein, K.-L., Chupp, E. L., Trotter, G., Magun, A., Dunphy, P. P., Rieger, E., & Urpo, S. 1999, *A&A*, 348, 271
 Kohl, J. L., et al. 1995, *Sol. Phys.*, 162, 313
 Lario, D. 2005, *Adv. Space Res.*, 36, 2279
 Maia, D., Pick, M., Vourlidas, A., & Howard, R. 2000, *ApJ*, 528, L49
 Malitson, H. H., Fainberg, J., & Stone, R. G. 1973, *Astrophys. Lett.*, 14, 111
 Mancuso, S., Raymond, J. C., Kohl, J., Ko, Y. K., Uzzo, M., & Wu, R. 2002, *A&A*, 383, 267
 Mann, G., Classen, T., & Aurass, H. 1995, *A&A*, 295, 775
 Mann, G., Klassen, A., Aurass, H., & Classen, H. T. 2003, *A&A*, 400, 329
 Nelson, G. J., & Melrose, D. B. 1985, in *Solar Radiophysics: Studies of Emission from the Sun at Metre Wavelengths*, ed. D. C. McLean & N. R. Labrum (Cambridge: Cambridge Univ. Press), 333
 Newkirk, G. J. 1961, *ApJ*, 133, 983

- Priest, E. R. 1982, *Solar Magnetohydrodynamics* (Dordrecht: Reidel)
- Raouafi, N.-E., Mancuso, S., Solanki, S. K., Inhester, B., Mierla, M., Stenborg, G., Delaboudinière, J. P., & Benna, C. 2004, *A&A*, 424, 1039
- Raymond, J. C., et al. 2000, *Geophys. Res. Lett.*, 27, 1439
- Reames, D. V. 1999, *Space Sci. Rev.*, 90, 413
- . 2000, in *AIP Conf. Proc.* 516, Invited, Rapporteur, and Highlight Papers, ed. B. L. Dingus, D. B. Kieda, & M. H. Salamon (New York: AIP), 289
- Reinard, A. A., & Andrews, M. A. 2006, *Adv. Space Res.*, 38, 480
- Robinson, R. D., & Stewart, R. T. 1985, *Sol. Phys.*, 97, 145
- Saito, K., Poland, A. I., & Munro, R. H. 1977, *Sol. Phys.*, 55, 121
- Schatten, K. H. 1971, *Cosmic Elettrodyn.*, 2, 232
- Schatten, K. H., Wilcox, W. J., & Ness, F. N. 1969, *Sol. Phys.*, 6, 442
- Schrijver, C. J., DeRosa, M. L., Title, A. M., & Metcalf, T. R. 2005, *ApJ*, 628, 501
- Sheeley, N. R., et al. 1997, *ApJ*, 484, 472
- Shen, C. I., Wang, Y. M., Ye, P. Z., & Wang, S. 2006, *ApJ*, 639, 510
- Vourlidas, A., Wu, S. T., Wang, A. H., Subramanian, P., & Howard, R. A. 2003, *ApJ*, 598, 1392
- Vršnak, B., Magdalenic, J., & Zlobec, P. 2004, *A&A*, 413, 753
- Warmuth, A., & Mann, G. 2005, *A&A*, 435, 1123
- Wild, J. P., & McCready, L. L. 1950, *Australian J. Sci. Res.*, A3, 387
- Zhao, X. P., & Hoeksema, J. T. 1992, in *Proc. First SOHO Workshop: Coronal Streamers, Coronal Loops, and Coronal and Solar Wind* (ESA SP-348; Garching: ESA), 117
- . 1994, *Sol. Phys.*, 151, 91
- . 1995, *J. Geophys. Res.*, 100, 19
- Zhao, X. P., Hoeksema, J. T., & Rich, N. B. 2002, *Adv. Space Res.*, 29, 411